Fabrication of spherical particles with mixed amorphous/crystalline nanostructured cores and insulating oxide shells

J.I. Hong[a)]
School of Materials Science and Engineering, Georgia Institute of Technology, Atlanta, Georgia 30126; and Center for Magnetic Recording Research, University of California—San Diego, La Jolla, California 92093

F.T. Parker
Center for Magnetic Recording Research, University of California—San Diego, La Jolla, California 92093

V.C. Solomon and P. Madras
School of Materials, Arizona State University, Tempe, Arizona 85287

David J. Smith
School of Materials and Department of Physics, Arizona State University, Tempe, Arizona 85287

A.E. Berkowitz
Center for Magnetic Recording Research and Department of Physics, University of California—San Diego, La Jolla, California 92093

(Received 14 September 2007; accepted 11 March 2008)

By spark-eroding $Fe_{75}Si_{15}B_{10}$ in water/ethanol mixtures, spherical particles with nanostructured cores consisting of mixed amorphous and crystalline phases were produced. The relative volume fractions of the amorphous and crystalline phases were dependent on the water/ethanol ratio. In the same process, continuous oxide layers were formed on the particle surfaces. The basic mechanisms responsible for the formation of the surface oxide layers and the core nanostructures were modeled. At frequencies ranging from 1 to 100 MHz, the combination of the core nanostructures and the insulating oxide shells yielded exceptionally low-loss magnetic behavior.

I. INTRODUCTION

Melt-spun ribbons with mixed nanostructured amorphous/crystalline phases are usually produced from Fe–Si–B alloys with some additional elements such as Cu, Nb, or Zr, followed by heat treatment.[1–3] In the present study, it is shown that spherical, nanostructured particles with mixed crystalline/amorphous phases can be formed directly from Fe–Si–B by spark-erosion[4,5] in water/ethanol mixtures without requiring post-annealing. The relative ratio of crystalline and amorphous phases is determined by the water/ethanol ratio used in the spark-erosion process. With water as the dielectric liquid, the spark-eroded particles consist of spherical amorphous nanoparticles in a crystalline matrix, a reversal of the usual situation. The amorphous fraction increases as ethanol is added to the dielectric liquid. A continuous, insulating oxide coating on these particles is produced with these dielectric liquids. It is shown how these features arise from the nature of the spark-erosion process and the Fe–Si–B alloy composition. The high temperature of the microplasmas involved in spark erosion, and the rapid in situ quenching in the dielectric liquid, are essential for producing the unique microstructure of these particles.

II. SYNTHESIS AND CHARACTERIZATION

A variation on the usual "shaker-pot" spark-erosion apparatus[3] was used. Two $Fe_{75}Si_{15}B_{10}$ alloy discs, 2 in. in diameter and 0.5 in. in thickness, were mounted at the ends of two parallel rotating axles, with the sidewalls of the discs facing each other, as shown in Fig. 1. The discs were immersed in a dielectric liquid, and a Hansvedt 1506 EDM power supply (Hansvedt EDM, Rantoul, IL) was used to apply voltage pulses with 1-μs width and 100-V amplitude at 200 kHz to the discs to produce sparks in the gap between them. The amplitude of the current peaks ranged from 10 to 15 A. The gap between the discs was maintained at ~1 μm with a stepping motor control of the position of one disc. Microplasma sparks between the discs were initiated when the electric field in the gap was large enough to produce a breakdown of the dielectric liquid. The temperatures within the spark/

[a)]Address all correspondence to this author.
e-mail: jhong@gatech.edu
DOI: 10.1557/JMR.2008.0199

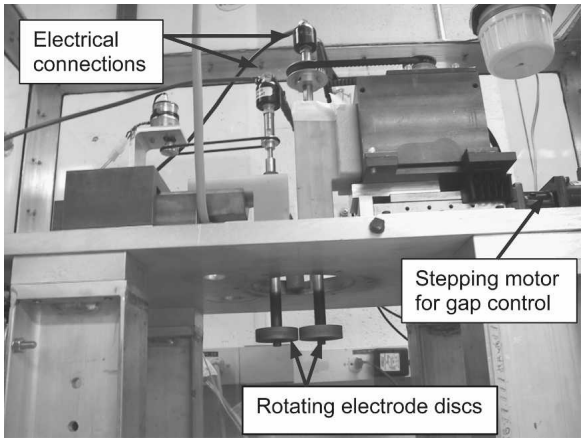

FIG. 1. Photograph of the rotating electrode spark-erosion system with Fe–Si–B disks mounted.

plasma region were on the order of 10^4 K. The kinetic energies of the electrons and positive ions in the spark were transferred to localized spots on the disc surfaces. These regions were superheated above their boiling temperatures by the spark energies due to the high pressure exerted by the surrounding incompressible dielectric liquid. When a spark collapsed, molten droplets were ejected from these localized boiling regions and were rapidly quenched in situ in the dielectric liquid.[4–6] Because erosion on the disc surface from each spark took place over a very small region, the surfaces of the discs remained smooth enough to keep the gap width approximately constant at ~1 μm, with periodic calibration effected by the stepping motor. The spark-eroded particles were washed several times with methanol and hexane, and dried under flowing nitrogen.

The microstructure of the particles was determined using x-ray diffraction (XRD) with Co K_α radiation, scanning electron microscopy (SEM) with an FEI (Hillsboro, OR) XL-30 microscope, and transmission electron microscopy (TEM) with a JEOL (Tokyo, Japan) JEM-4000 EX microscope. The scanning electron microscope was equipped with an energy-dispersive x-ray spectrometer, which was used to determine composition profiles across cross sections of polished particles. Magnetic hysteresis loops were measured with a vibrating-sample magnetometer at room temperature. The frequency response up to 100 MHz was measured on cylinders, 3 mm in diameter and 10 mm in length, prepared from mixtures of the particles with epoxy. The impedance of a coil wound around the cylindrical sample was measured for this latter purpose.

III. RESULTS

The particles were primarily spherical with diameters <5 μm, as shown by the scanning electron micrograph in Fig. 2, with the majority having sizes in the range of 1–3 μm. The average size could be controlled by adjusting the amplitude of the current peak.[4,5] Figure 3 shows XRD spectra for particles that were spark-eroded in water/ethanol mixtures with different relative concentrations. Each spectrum consists of superimposed broad and sharp lines, corresponding to the presence of amorphous and crystalline phases, respectively. The XRD spectrum of completely amorphous Fe–Si–B particles, prepared by spark erosion in dodecane ($C_{12}H_{26}$), is included for comparison.[7] The four well-defined peaks in these spectra correspond to the body-centered cubic α-phase of an Fe–Si alloy.[8] The intensities of these crystalline peaks are roughly proportional to the water concentration in the dielectric liquid and inversely proportional to the amorphous peak intensities. The broad lines in the spectra can clearly be identified with the amorphous Fe–Si–B phase produced by spark erosion in dodecane.

The relative fractions of crystalline and amorphous phases in the particles were derived from the ratio of the integrated intensities of the crystalline and amorphous peaks. Exact scaling between the integrated intensity and

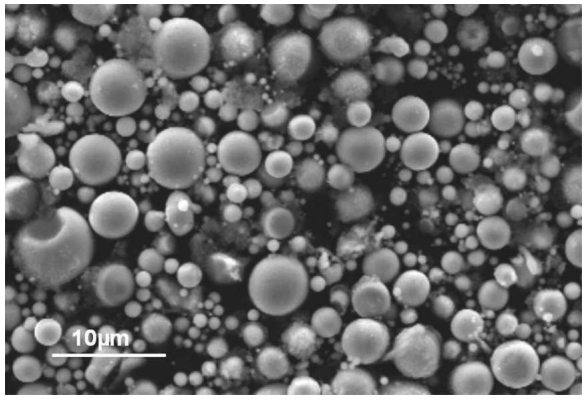

FIG. 2. SEM micrograph showing spherical particles spark-eroded in a water/ethanol (50:50) mixture.

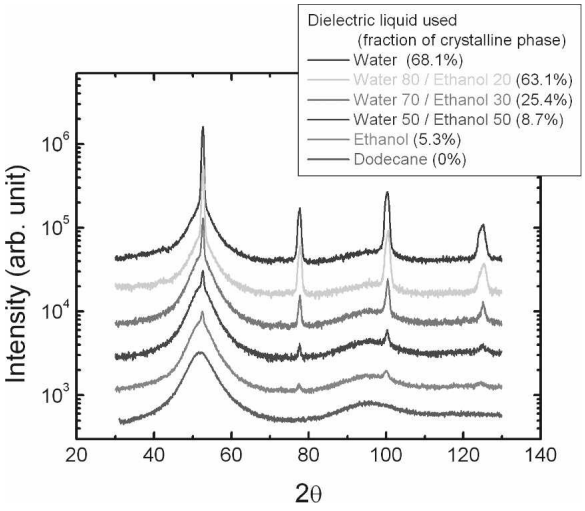

FIG. 3. XRD spectra of Fe–Si–B particles spark-eroded in different water/ethanol mixtures, indicating different proportions of crystalline and amorphous phases. The spectra are ordered as indicated in the inset.

the fraction of the corresponding phase present in the specimen was obtained by measuring the XRD spectrum of Fe–Si–B particles that were spark-eroded in water and another XRD spectrum taken from a mixture of crystalline and amorphous Fe–Si–B particles with a known ratio of the phases. The resulting calculated fraction of crystalline phase in the particles increased with the relative water concentration in the dielectric liquid, as indicated in the inset of Fig. 3.

The microstructure and morphology of the particles were determined from TEM and SEM micrographs. The TEM micrograph in Fig. 4(a) shows that particles spark-eroded in water consist primarily of amorphous nanoparticles (indicated by "P") distributed in a crystalline matrix (indicated by "M"). This arrangement is the reverse of the usual microstructure for systems with mixed amorphous and crystalline phases.[1,2] High-resolution imaging revealed the respective amorphous and crystalline regions, and the selected-area electron-diffraction patterns shown in the insets in Fig. 4(a) also confirm the amorphous and crystalline microstructure of the particles and matrix, respectively. Particles spark-eroded in ethanol have a very different microstructure and morphology. The TEM micrograph in Fig. 4(b) of a particle spark-eroded in ethanol shows darker crystalline regions that are separated by amorphous channels having lighter contrast.

SEM micrographs of cross sections of particles spark-eroded in water are shown in Figs. 5(a) and 5(b). These particles were fixed in epoxy and mechanically polished to expose their cross sections. As shown in Fig. 5(b), the x-ray microanalysis profiles across the outer shells of the particles confirm that the surfaces of these particles were enriched with oxides of boron and silicon.

The formation of crystalline or amorphous phases in the spark-eroded particles depends primarily on the quenching rate of the molten droplets produced by the sparks. The quenching rate, in turn, is determined by the heat capacity or volatility of the dielectric liquid. For an organic liquid with a relatively high molecular weight, such as dodecane, the interface between the molten droplets and the dielectric presumably remains liquid. Thus, the quenching rate is very rapid, yielding amorphous $Fe_{75}Si_{15}B_{10}$ particles. With ethanol, which is much more volatile, in the dielectric, the molten-droplet/dielectric interface is more likely to consist of a vapor

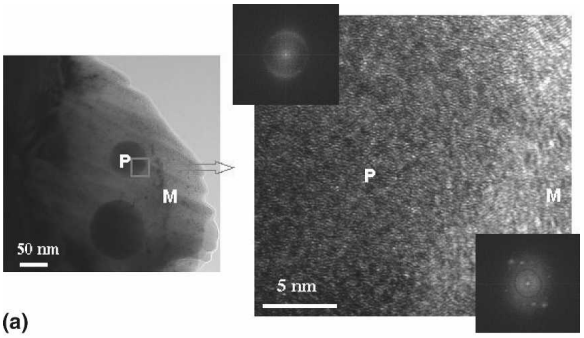

(a)

(b)

FIG. 4. TEM micrographs of Fe–Si–B particles: (a) spark-eroded in water (insets are selected-area electron-diffraction patterns of an amorphous nanoparticle and the crystalline matrix); and (b) spark-eroded in ethanol. Note the amorphous channels (lighter contrast) separating the crystalline regions.

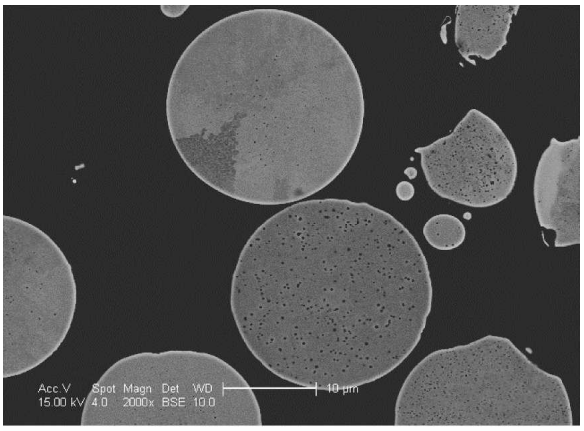

(a)

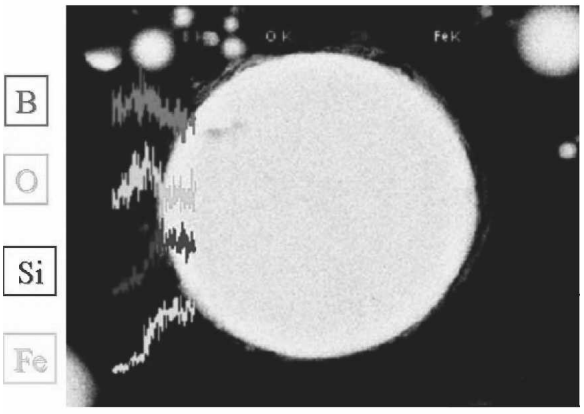

(b)

FIG. 5. SEM micrographs of cross sections of particles spark-eroded in water after mechanical polishing. White rings corresponding to oxide surface layers are visible in (a), and variations in local chemical composition indicated by small-probe x-ray microanalysis profiles are shown in (b).

sheath. Heat transfer out of the droplets through the vapor sheath will be slower, permitting crystalline phases to be established.

The microstructure of the particles and the elemental distribution within them are strongly influenced by the composition of the dielectric. With water or ethanol in the dielectric, oxygen becomes available, which enables the formation of oxide coatings on the particles. The coating is identified as mostly boron oxide, as expected, because boron in Fe–Si–B has the greatest affinity for oxygen. Moreover, the fact that some boron becomes oxidized reduces the fraction of boron retained in the particle cores. Because the presence of adequate boron is essential for the formation of amorphous Fe–Si–B, some crystalline Fe–Si phase will be present in the cores, as was observed.

The chemical/microstructural behavior of boron in these particles was further confirmed by the spark erosion of alloys with a higher B concentration. The objective was to retain enough B in the particle cores to result in an amorphous Fe–Si–B core with a B-rich oxide shell. The B concentration was increased by 3%, while keeping the Fe/Si ratio constant. Accordingly, $Fe_{72.5}Si_{14.5}B_{13}$ was spark-eroded in ethanol at the same power setting previously used for $Fe_{75}Si_{15}B_{10}$. The XRD spectra for the two materials after spark erosion are compared in Fig. 6. Clearly, by ensuring adequate boron content in the cores, the increased B content in $Fe_{72.5}Si_{14.5}B_{13}$ has resulted in suppression of the small fraction of the crystalline phases that was present when $Fe_{75}Si_{15}B_{10}$ was spark-eroded in ethanol.

Boron segregation at the particle surfaces as a function of particle size was examined by spark-eroding $Fe_{75}Si_{15}B_{10}$ at high power using the shaker-pot apparatus in a water–ethanol (50:50) mixture to produce particles with sizes ranging from submicron to 30 μm.[3,4] The particles were classified by size, and the corresponding XRD spectra are shown in Fig. 7. The smaller particles have greater fractions of crystalline phase [Fig. 7(a)], and the lattice constant of their crystalline phase is larger [Fig. 7(b)]. As the particle diameter decreases, the surface/volume ratio increases. Therefore, larger fractions of B and Si are consumed by the formation of surface oxide layers in the smaller particles. The consumption of B in the oxide shells yields higher fractions of the crystalline phase in the particle cores. The consumption of some Si in the oxide shell results in the slightly larger average lattice constant of the crystalline phase due to the lower Si concentration in the corresponding Fe–Si alloy.

Figure 8 shows the saturation magnetization (σ_S) and the coercivity (H_C) of the particles. σ_S increased as the water concentration increased, due to the increased concentration of the crystalline Fe–Si alloy. The H_C of the

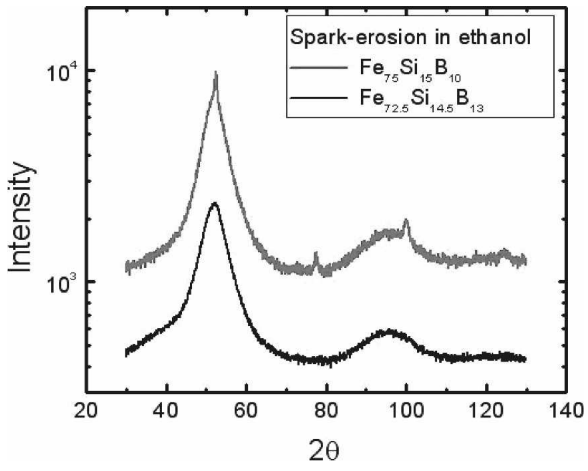

FIG. 6. XRD spectra for Fe–Si–B particles spark-eroded in ethanol using starting alloys with different concentrations, as indicated. The Fe/Si ratio was kept constant for both alloys, while the B concentration was increased by 3%.

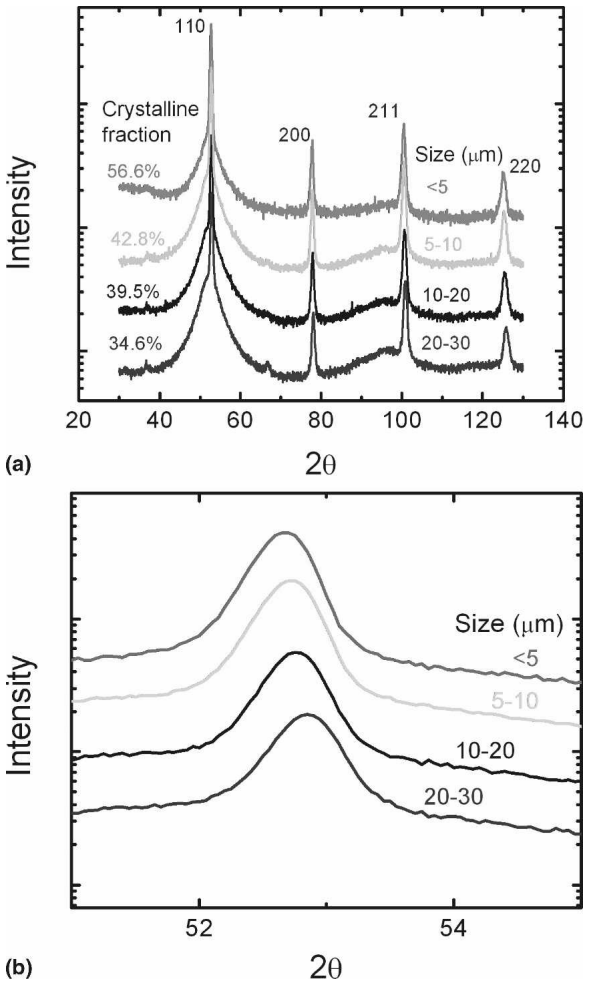

FIG. 7. XRD spectra of Fe–Si–B particles spark-eroded with high power and a large gap to produce particles of various sizes ranging up to ~30 μm. (a) Particles classified by sieving; and (b) magnified view of the 110 peaks shows that the peak position shifts slightly depending on the average particle size.

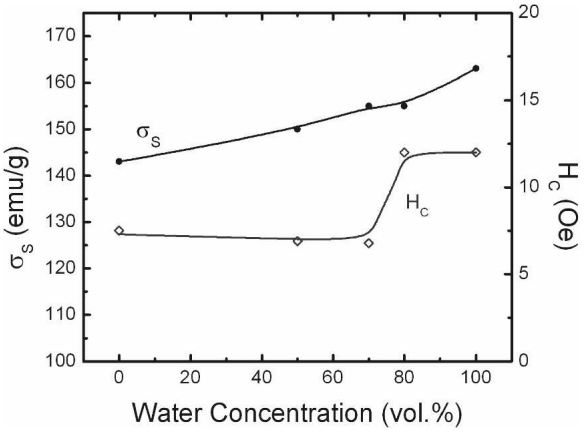

FIG. 8. σ_S and H_C as functions of water concentration in the water/ethanol dielectric liquid.

particles remained at ~7 Oe for water concentrations up to ~70 vol%, and then increased somewhat abruptly to ~12 Oe for water concentrations between 70 and 80 vol%. These results suggest that H_C is determined by the concentration of the crystalline phase in the particles, which is indicated by the XRD analysis in Fig. 3. Thus, with up to 70% water in the dielectric liquid, the minor crystalline Fe–Si phase fraction increases only slowly, but the transition from predominantly amorphous to mostly crystalline phase occurs principally between 70% and 80% water content. H_C is also influenced by the different microstructures of the particles spark-eroded in water and ethanol, as shown in Fig. 4. The particles spark-eroded in water consist of amorphous nanoparticles in a crystalline matrix The amorphous nanoparticles can serve as pinning sites for domain walls, thereby increasing H_C. The particles spark-eroded in ethanol are composed of amorphous channels separating crystalline regions, as seen in Fig. 4(b). This microstructure approaches the distribution of nanophases smaller than the magnetic exchange length, thereby averaging out their magnetocrystalline anisotropy, as described by Herzer.[1] We note that the values of H_C for these particles are considerably larger than those of amorphous or Finemet ribbons, which generally have coercivities <1 Oe. As discussed above, the difference in the microstructures of the spark-eroded particles and the amorphous and Finemet ribbons is the principal reason for the higher H_C of the particles.

The insulating oxide shells on the particles suggested that lower losses might be anticipated at high frequencies. Accordingly, cylindrical rods for *ac* measurements were prepared from composites of the particles with epoxy at various particle volume fractions. The inductance of a coil was measured from 1 to 100 MHz with and without insertion of these rod samples, and the permeabilities μ' and μ'' were obtained from the inductance. Because magnetic flux lines do not close with rod samples, the values of μ' and μ'' were only relative measures. However, it was confirmed that a reliable comparison could be made between the composites made from various particle mixtures using the rods. The permeabilities of the composite rods were compared with the permeabilities of toroids made from the same particle–epoxy mixtures for several different kinds of particles. The permeabilities of the toroid samples were approximately two times larger than the values measured with rod-shaped samples. Furthermore, both types of samples showed the same trend in permeability, which depended on the microstructure of the particles, and on their concentration in the composite. This behavior confirmed the validity of the measurements on the rods for a comparative study of the high-frequency magnetic properties of the particles.

The values of μ' and μ'' at 50 MHz are plotted in Fig. 9 as functions of the particle volume fraction in the polymer composites for amorphous particles spark-eroded in dodecane without the oxide shell, and for

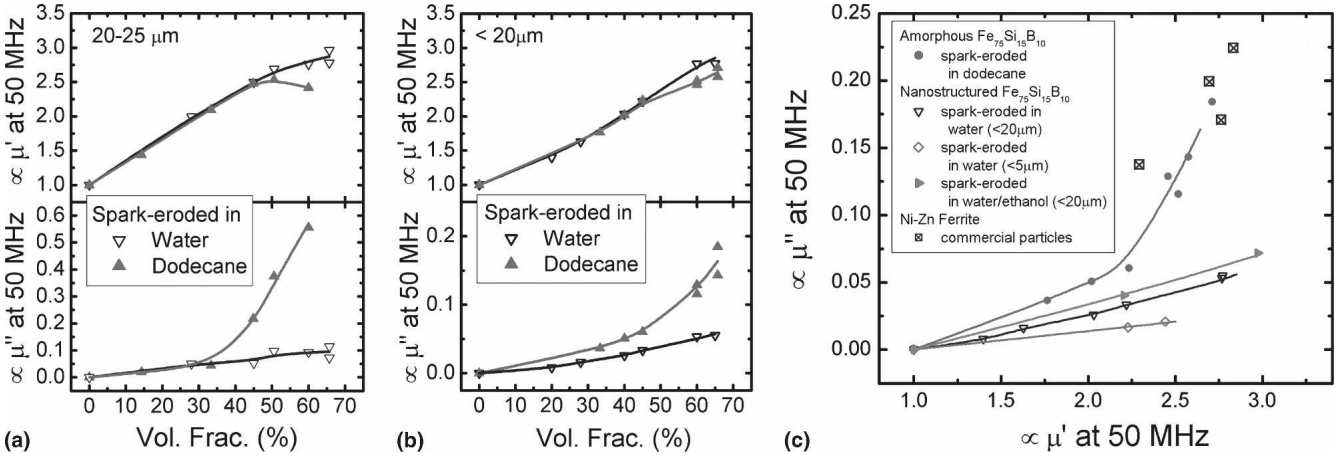

FIG. 9. Permeabilities measured at 50 MHz for composites of particles: (a) 20–25 μm and (b) <20 μm, as prepared in dodecane and in water, as functions of particle concentrations; and (c) μ'' versus μ' for composites made from various particles. Composites made with NiZn ferrite particles are included for comparison.

oxide-coated particles with mixed amorphous/crystalline microstructure. At all concentrations, the particles spark-eroded in water exhibited equal or higher μ' and lower μ'' (lower loss) than the amorphous particles. With the amorphous particles, μ'' increased abruptly when the particle concentration was above the percolation limit and significant currents appeared. This increase of μ'' is particularly evident for particles 20–25 μm in size with volume fractions greater than ~40%, at which point μ' decreases. The decrease in μ' occurs with the onset of interparticle conduction, because the high currents surrounding groups of these particles will screen them, thereby decreasing the effective net volume of magnetic particles in the composite. The interparticle currents for amorphous particles <20 μm in size are smaller because of the increased density of the interfaces; this produces lower screening of groups of particles. This behavior can also be visualized as resulting from an effective skin depth that is lower for smaller percolating particles by virtue of their higher effective resistivity due to more interparticle contacts.

Particles spark-eroded in water, with insulating oxide coatings, do not exhibit interparticle conduction at percolation. As shown in Fig. 9, the μ' for these particles increased in proportion to the particle volume fraction up to the maximum volume fraction tested (65%), without an abrupt increase in μ''. The surface oxide coatings that formed during spark erosion in water prevent interparticle conduction. Therefore, a low loss level is maintained with high electrical resistance between neighboring particles, even at particle volume fractions above the percolation limit.

Figure 9(c) shows values of μ'' plotted against values of μ' for composites made from four different kinds of particles. Each line in the figure corresponds to composites made from one type of particle with increasing particle concentrations. As the particle volume fraction in the composite increases, the μ' and μ'' values increase following the lines corresponding to the particle of interest. For the composite made of amorphous $Fe_{75}Si_{15}B_{10}$ particles without an oxide coating, there is a linear relationship between μ' and μ'' until percolation produces the abrupt change of slope. A low constant slope means that the composite made of those particles can reach higher μ' with a low loss level. Therefore, comparisons among different particles can be readily made from this plot of μ'' versus μ'. The composites of $Fe_{75}Si_{15}B_{10}$ particles spark-eroded in water with sizes <5 μm exhibit the best properties of high μ' and low μ'', as indicated by the lowest line in Fig. 9(c). The μ'' value is lower, by more than an order of magnitude, than the corresponding values for amorphous $Fe_{75}Si_{15}B_{10}$ or for commercially available Ni–Zn ferrites. Although ferrite composites exhibit superior performance at lower frequencies (in the kilohertz range), their performance degrades rapidly as the applied frequency is increased up to the megahertz range. This is in contrast to the oxide-coated nanostructured $Fe_{75}Si_{15}B_{10}$ particles, which retain their permeability up to the maximum frequency tested in the present study.

IV. CONCLUSION

Spark erosion of Fe–Si–B with water/ethanol mixtures used as the dielectric liquid produces spherical particles with a nanostructure consisting of amorphous and crystalline phases without requiring any postheating treatment. With water as the dielectric liquid, the particles have a crystalline matrix in which amorphous nanoparticles are distributed, opposite the usual amorphous–crystalline microstructure. The amorphous/crystalline ratio increases as the ethanol fraction increases, and the microstructure becomes one of amorphous channels separating crystalline nanoregions. Moreover, these particles have insulating oxide coatings, composed primarily of the readily oxidized boron. The dc magnetic properties reflect the microstructure of the particles, and the high-frequency properties in the range of 1–100 MHz strongly benefit from the insulating coating. The oxide coating permits a particle-packing density above the percolation limit with no penalty for unacceptable losses. The present study focused on Fe–Si–B compositions. However, it should be noted that oxide-coated spherical particles with virtually any composition can be prepared in one step by spark erosion in a dielectric liquid containing some oxygen. It is only necessary that the starting material contains a small amount of a readily oxidized element.

ACKNOWLEDGMENT

The authors acknowledge the use of facilities in the John M. Cowley Center for High Resolution Electron Microscopy at Arizona State University.

REFERENCES

1. G. Herzer: Nanocrystalline soft magnetic materials. *J. Magn. Magn. Mater.* **112,** 258 (1992).
2. M.E. McHenry and D.E. Laughlin: Nano-scale materials development for future magnetic applications. *Acta Mater.* **48,** 223 (2000).
3. A. Inoue: Stabilization of metallic supercooled liquid and bulk amorphous alloys. *Acta Mater.* **48,** 279 (2000).
4. A.E. Berkowitz and J.L. Walter: Spark erosion: A method for producing rapidly quenched fine powders. *J. Mater. Res.* **2,** 277 (1987).
5. J. Carrey, H.B. Radousky, and A.E. Berkowitz: Spark-eroded particles: Influence of processing parameters. *J. Appl. Phys.* **95,** 823 (2004).
6. D.D. DiBitonto, P.T. Eubank, M.R. Patel, and M.A. Barrufet: Theoretical models of the electrical discharge machining process: I. A simple cathode erosion model. *J. Appl. Phys.* **66,** 4095 (1989).
7. A.E. Berkowitz, J.L. Walter, and K.F. Wall: Magnetic properties of amorphous particles produced by spark erosion. *Phys. Rev. Lett.* **46,** 1484 (1981).
8. R.M. Bozorth: *Ferromagnetism* (Van Nostrand, New York, 1951).